International Journal of GEOMATE, May 2019, Vol.16, Issue 57, pp.82 - 88
Geotec., Const. Mat. & Env., DOI: https://doi.org/10.21660/2019.57.4722
ISSN: 2186-2982 (Print), 2186-2990 (Online), Japan

NON-CONTACT ESTIMATION OF STRAIN PARAMETER-TRIGGERING LIQUEFACTION

*Erica Elice S. Uy[1], Toshihiro Noda[2], Kentaro Nakai[3,] and Jonathan R. Dungca[4]

[1,4] Department of Civil Engineering, College of Engineering, De La Salle University, Philippines
[2,3] Department of Civil and Environmental Engineering, School of Engineering Nagoya University, Japan

*Corresponding Author, Received: 11 Nov. 2018, Revised: 15 Dec. 2018, Accepted: 30 Dec. 2018

ABSTRACT: The strain parameter-triggering liquefaction is usually determined by implementing cyclic strain approach with a corresponding laboratory experiment. These parameters are threshold shear strain, cyclic shear strain and cyclic shear strain that would trigger liquefaction. In this study, non-contact measurement technique was implemented to estimate and monitor the development of the mentioned parameters. In this technique, a mirrorless camera and Lucas and Kanade pyramidal optical flow algorithm were utilized to track the movement of the particles. The camera was first calibrated to eliminate the errors from the lens and the scene as well. Furthermore, curvature correction was applied because the sample tested has a curved profile. The comparison was made with the loose and medium dense conditions. The samples were tested under a consolidated undrained cyclic triaxial test at 2.4, 1.6 and 0.8 mm strain amplitudes. The confining pressures used were 50, 100 and 200 kPa. Based on the results, a non-contact measurement technique can estimate the parameters. A range of values was established due to the non-homogeneous movement of the soil.

Keywords: Cyclic Loading, Non-Contact Measurement, Strain Parameter-Triggering Liquefaction, Curvature Correction

1. INTRODUCTION

Liquefaction assessment is performed to determine the vulnerability of the soil to liquefy [1]. Assessment can be performed by cyclic stress approach or cyclic strain approach. In these approaches, parameters needed are obtained from in-situ testing techniques or laboratory testing [2]-[3]. The cyclic stress approach considers the build-up of pore water pressure related to the cyclic shear stress (τ_c). Several studies pointed out that the results of this approach are dependent on the overconsolidation ratio (OCR), shaking effect, lateral earth pressure coefficient (K_0), relative density and method of sample preparation [2]-[3]. Due to this, researchers are focused on utilizing the cyclic strain approach. In this approach, the cyclic shear strain is being correlated to the excess pore water pressure. Since it can characterize particle rearrangement. The cyclic shear strain is associated with the deformation of the particles which is a result of ground shaking [4]. This can produce excess pore water pressure which can result in liquefaction. Strain parameter-triggering liquefaction is used in the assessment. The parameters are threshold shear strain (γ_{tv}), cyclic shear strain (γ_c) and cyclic shear strain that would trigger liquefaction (γ_{cl}). The γ_{tv} is the indicator of the initiation of development of pore water pressure in a cyclic test. This parameter is approximately $1x10^{-2}$% existing for clean sand as seen in Fig. 1 [2]-[3].The γ_{cl} is the parameter compared to γ_c on the triggering of liquefaction. When γ_c exceeds the value of γ_{cl} this implies that triggering of liquefaction had occurred. Its typical value ranges from 0.4 to 3% [3]. The minimum value of this parameter can also be seen in Fig. 1. At this point, the pore water pressure ratio is almost 0.95. The strain parameter-triggering liquefaction is normally obtained from field tests or laboratory tests such as cyclic simple shear test and dynamic triaxial test. In these tests, the Linear Variable Displacement Transducer (LVDT) is used to determine these parameters. Kaddouri (1991) installed the LVDT inside the triaxial cell in order to address the non-homogeneous deformations measured by Dobry et al. (1981-1982) and Youd (1972) [5]. This set-up can cause disturbances to the sample especially on how it is attached. It is also susceptible to the tilting of the sample which can lead to errors in measurement. Furthermore, this set-up cannot monitor the development of the strain parameter-triggering liquefaction. A method that can be implemented is a non-contact measurement technique. It utilizes cameras to estimate the deformation of an object without causing any disturbances [6]. Deformations are estimated through image processing algorithms such as digital image correlation (DIC), particle image velocimetry (PIV) and optical flow [6]-[8]. The technique can provide local deformation, monitor the material's behavior during the experiment and assess the actual test boundary condition. The technique was applied

in a cyclic triaxial test. Based on the results, the technique has the capacity to measure the development of deformation [7]-[8]. In this study, non-contact measurement technique was used to estimate and monitor the strain parameter-triggering liquefaction. Two-dimensional image processing was implemented. Lucas and Kanade pyramidal optical flow algorithm were used to track the deformation. A mirrorless camera was used because it is more economical compared to a single lens reflex (SLR) camera or a high-speed camera. The strain-controlled consolidated undrained test was performed for a loose and medium dense condition.

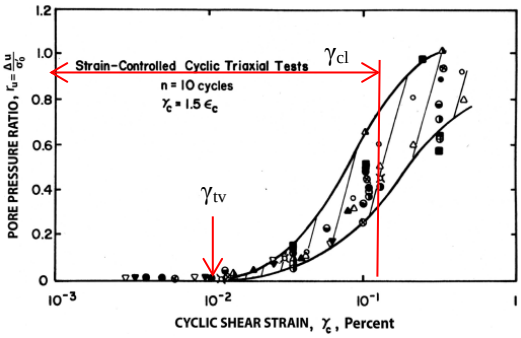

Fig.1 Pore water pressure ratio plotted against γ_c [3]

2. NON-CONTACT MEASUREMENT

2.1 Calibration

The non-contact measurement was carried out by using a mirrorless camera and optical flow algorithm. The camera was initially calibrated and it is divided into two phases. In the first phase, a calibration grid, as seen in Fig. 2a, with uniform dimension and spacing, was used as a target to extract the internal and external camera parameters. These parameters were used to determine the position of the points with respect to the camera coordinate system. This was followed by applying the polynomial distortion model to correct the distortion from the lens. In the second phase, a magnification factor was determined. This was to eliminate the magnification from the triaxial cell and water. Measurements were made using a straight edge block, Fig. 2b. It was carried out by placing the straight edge block in the triaxial cell and it was submerged with water. It can be seen that rectangular targets were also placed on the block. Different sizes were used to determine the amount of magnification encountered. The dimension of the block is 10.0 cm x 7.0 cm. The dimensions of the targets are tabulated in Table 1. A straight edged block and rectangular targets were also used in order to have an easy detection of the dimensions. Edge detection was the image processing method used to determine their dimensions. In order to determine the magnification factor, the actual dimension was plotted against the measurement from image processing. The slope of the plot is the magnification factor. The values obtained were 0.7036 and 0.8579 for the x and y-directions, respectively. During this phase, the camera settings and the exact location of the camera were determined. In order to ensure that the position of the camera was fixed, it was placed at the back of the equipment. It was placed 42 cm from the equipment. In this location, the camera will not be disturbed during the duration of the experiment. Lighting was also controlled in order to avoid noise from uneven lighting. The area where uneven light penetrated was covered with black paper. Furthermore, a spot light was placed to improve the distribution of light.

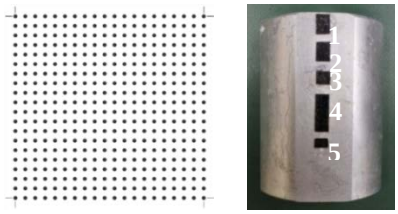

(a) (b)

Fig.2 Calibration tools (a) calibration grid (b) straight edge block

Table 1 Dimension of the targets

Target	Dimension (LxH) (cm)
1	0.7x1.0
2	0.7x1.0
3	0.7x0.7
4	0.7x2.0
5	0.7x0.5

2.2 Curvature Correction

The samples tested were in a cylindrical shape. Since only 2D image processing was implemented in the study the curvature effect needs to be corrected. The images of the sample were corrected using the polynomial model. This model is usually applied in a geometric correction since it can correct more complicated types of distortion such as curved surfaces [9]. The model is also known as nonlinear transformation equation and it has the following expression:

$$\mathbf{x'} = \mathbf{a_0} + \mathbf{a_1 x} + \mathbf{a_2 y} + \mathbf{a_3 x^2} + \mathbf{a_4 xy} + \mathbf{a_5 y^2} \quad (1)$$

$$\mathbf{y'} = \mathbf{b_0} + \mathbf{b_1 x} + \mathbf{b_2 y} + \mathbf{b_3 x^2} + \mathbf{b_4 xy} + \mathbf{b_5 y^2} \quad (2)$$

where x' and y' = corrected real-world coordinates in x- and y-axis; x and y = original real-world coordinates in x- and y-axis; a_0 to a_5 and b_0 to b_5 = polynomial correction parameters. The parameters were obtained by the least square error method for each experiment.

In order to validate the model applied, corrected deformation readings were compared to the LVDT. The target points chosen are shown in Fig. 3. These

points were chosen since it is independent of the soil movement. The displacement of the soil based on the results can be smaller or larger than the LVDT. The typical results are shown in Figs. 4-5. It is noticeable that the rightmost side experienced more curvature than the leftmost side. It can be seen on the extension loading of the rightmost side of the displacements from image processing (IP) were smaller. Applying the curvature correction lessened the errors from IP. The errors at the left target lessened from 0.14 - 34.32% to 0.10 - 29.81%. For the right target, it lessened from 0.133 -37.671% to 0.031 - 29.236%. Based on these results, the polynomial model was adopted to correct the curvature present in the sample. In addition to the calibration previously discussed, curvature correction was always implemented prior to determining the deformation and strain parameter-triggering liquefaction. A correction was done with respect to the height of the sample, location, and section being monitored.

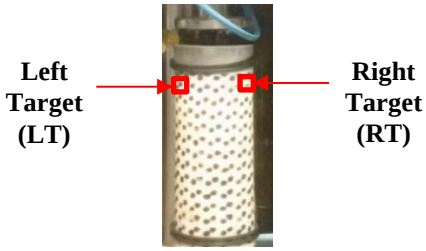

Fig.3 Monitored targets for curvature correction

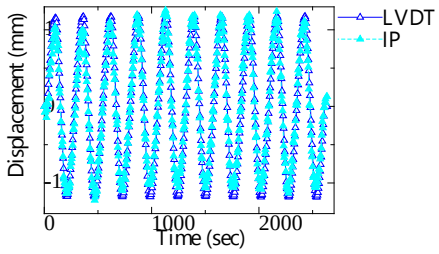

(a)

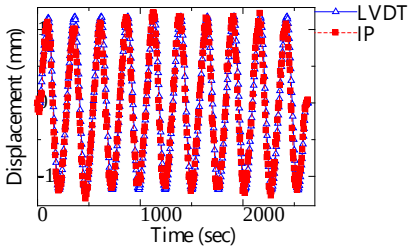

(b)

Fig.4 Monitored LT (a) not corrected (b) corrected

2.3 Optical Flow

Lucas and Kanade pyramidal optical flow algorithm were implemented to estimate monitor the movement of the soil under cyclic loading. The algorithm determines the image displacement ($\vec{d}$) of the point of interest by tracking it in succeeding grayscale images. It is a type of feature based approach where it assumes that brightness is ca onstant variable in the successive images. The algorithm uses image patches together with windowing methods. Least squares technique is implemented to extract the changes in position [11]. The residual function $\boldsymbol{\varepsilon}$ is minimized to extract the $\vec{d}$ [10].

$$\varepsilon(\vec{d}) = \varepsilon(d_x, d_y) = \sum_{x=u_x-\omega_x}^{u_x+\omega_x} \sum_{x=u_y-\omega_y}^{u_y+\omega_y} [I(x,y) - J(x+dx, y+dy)]^2 \quad (3)$$

where I(x, y) = First image with (x,y) pixel location; J(x, y) = Second image with (x,y) pixel location; dx, dy = image displacement and ω_x, ω_y = are arbitrary numbers that ranges from 1, 2, 3 or more pixels.

3. CYCLIC TRIAXIAL TEST

3.1 Sample Preparation

Mikawa number 6 sand was used in the study. It is an artificially produced shaved sample which has high concentrations of silica. It can be considered as silica sand and can be classified as a coarse material. This makes it susceptible to liquefaction. Samples were prepared by air pluviation as specified in the Japanese Geotechnical Society (JGS) standard for sample preparation of coarse granular materials for the triaxial test (JGS 0530-2009) [12]. Loose condition (S1) and medium dense (S2) were prepared to have 30% and 50% as the target relative density, respectively.

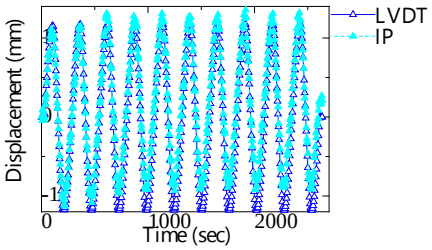

(a)

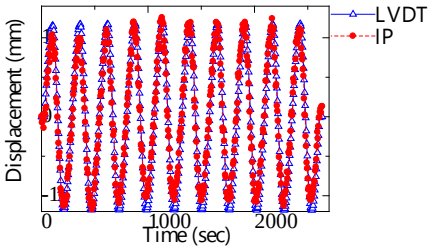

(b)

Fig.5 Monitored RT (a) not corrected (b) corrected

3.2 Cyclic Triaxial Test

The strain-controlled consolidated undrained test was performed as specified in the JGS 0541-2009 [12]. The confining pressure applied was 50, 100 and 200 kPa. The samples were cyclically loaded with 2.4, 1.6 and 0.8 mm strain amplitudes (SA) for 10 cycles. In order to properly estimate the strain parameter-triggering liquefaction, a slow frequency was adopted. Furthermore, images were taken every 5 seconds.

4. STRAIN PARAMETER-TRIGGERING LIQUEFACTION

The strain parameter-triggering liquefaction was estimated using the general engineering shear strain. Equation 4 was used in the computation [13]. The γ_c was first computed. The γ_{tv} and γ_{cl} were determined in correlation with the pore water pressure ratio. This is the ratio of the excess pore water pressure with the confining pressure. The γ_{tv} has a pore water pressure ratio close to zero or less than 0.1. At this point, there is no development of pore water pressure. The γ_{cl}, on the other hand, has a value close to 0.95. At this point, the triggering of liquefaction is about to occur. In order to apply Eqn 4, a 5 x 5-pixel rectangular grid was used in the estimation.

$$\gamma = \frac{1}{2}\left(\frac{\partial v}{\partial x} + \frac{\partial u}{\partial y}\right) \quad (4)$$

where $\frac{\partial v}{\partial x}, \frac{\partial u}{\partial y}$ = displacement gradient.

The cyclic shear strain that would trigger liquefaction was monitored at in three locations namely, left (L), center (C) and right (R) location. These locations are further subdivided into the top (T), middle (M) and bottom (B) section as seen in Fig. 6. The parameter was monitored at different locations and sections in order to investigate the occurrence of non-homogeneous deformation. The results estimated from IP were compared to the LVDT. Shear strain from LVDT was computed based on the following equation [14]:

$$\gamma = \varepsilon_a(1+\nu) \quad (5)$$

where ε_a = axial strain; ν = Poisson's ratio. The Poisson's ratio for saturated sand can be assumed to be 0.5.

5. RESULTS AND DISCUSSION

In order to verify the strain parameter-triggering liquefaction from the mirrorless camera, its measurements were compared with the LVDT. The LVDT used in the experiment had a rated capacity of 20 mm, a sensitivity of 5 mV/V ±0.1 % and measurement uncertainty of within ±0.1 % of its rated capacity. The comparison was made by choosing a target on the cyclic triaxial equipment. The target used was the top cap. Based on the results as seen in Fig. 7, there was a good agreement between the LVDT and IP. For the internal measurements, the monitored sections are similar to Fig. 6. It can be observed in Fig. 8 that there is an increasing amount of deformation as the monitored section is closer to the top cap or where there is direct contact with the applied load. Once liquefaction occurred it was observed that larger deformation was seen at the top section. The measurement from IP shows that deformation trend at different locations of the sample was not similar. This implies that non-homogeneous deformation exists during cyclic loading. The results of the strain parameter-triggering liquefaction are tabulated in Tables 2-5. Based on the results, a range of values was estimated due to the non-homogeneous movement observed from the locations and sections monitored. The estimated γ_{tv} was observed to have no consistent trend. It was observed that the minimum values estimated for both conditions are in the vicinity of 10^{-2}%. The results were compared to the typical values. It is consistent with the findings of Dobry and Abdoun (2011) that γ_{tv} in sands are in the order of 10^{-2}% or it is approximately $1x10^{-2}$% [2]-[3]. The maximum values, on the other hand, had larger results. This can be caused by the honeycombs present in the sample.

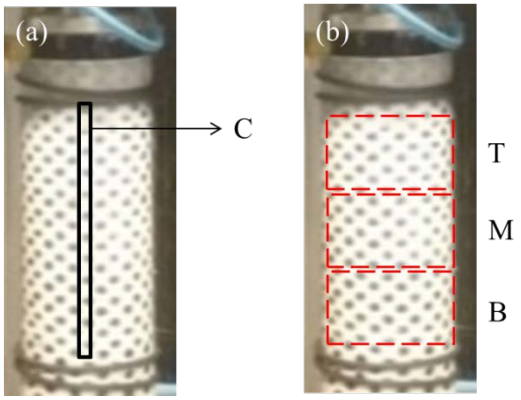

Fig.6 Monitored (a) location and (b) section

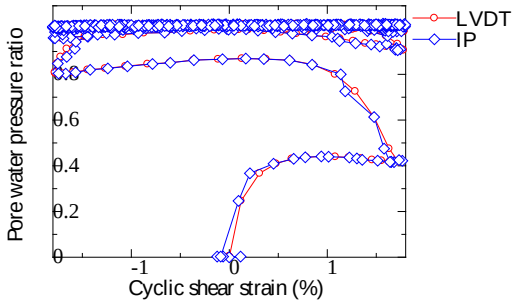

Fig.7 Comparison of the γ_c determined from LVDT and IP

Table 2 γ_{tv} for S1 (%) estimated from IP

SA	Loc	Cell Pressure (kPa) 50	100	200
2.4	T	0.0144-0.2948	0.0076-0.4225	0.0555-0.2619
	M	0.0265-0.3052	0.0020-1.0482	0.0066-0.6288
	B	0.0037-0.5131	0.0014-1.6852	0.0102-0.4843
1.6	T	0.0053-0.7529	0.0072-0.4165	0.0005-0.2751
	M	0.0008-0.8727	0.0324-0.6011	0.0001-0.2716
	B	0.0005-0.4789	0.0172-0.6765	0.0001-0.2045
0.8	T	0.0033-0.6206	0.0011-0.4505	0.0110-0.6521
	M	0.0014-0.8610	0.0015-0.5076	0.0077-0.5745
	B	0.0349-0.8843	0.0004-0.3942	0.0053-0.3090

A similar trend was observed when the IP results were compared with the LVDT results. The LVDT results are tabulated in Table 6. For the γ_{cl}, the effect of varying the relative density, strain amplitude and confining pressure was investigated. For the relative density, S1 had larger results compared to S2 since it has more voids present. Particle movement was more evident for S1. For the effect of strain amplitude, γ_{cl} had larger values for 2.4 mm SA. On the other hand, γ_{cl} decreased as the applied SA was smaller. The variation in the results was due to the difference in the applied amount of cyclic deformation. For the effect of increasing the confining pressure, the values for S1and S2 for all sections and locations decreased as the confining pressure was increased. As a whole, the estimated γ_{cl} from IP was observed to be affected by the relative density, strain amplitude and confining pressure.

Table 3 γ_{cl} for S1 (%) estimated from IP

SA	Loc	Cell Pressure (kPa) 50	100	200
2.4	T	1.6099-2.8610	1.3085-2.9153	0.6401-1.6863
	M	0.6910-4.5103	0.5722-2.8932	0.0047-0.9335
	B	0.0039-1.8144	0.0178-1.8413	0.0114-0.6625
1.6	T	0.2668-2.4369	0.6478-2.3364	0.6681-1.7113
	M	0.0567-1.8868	0.3210-1.8244	0.1803-1.4358
	B	0.0064-3.7311	0.0150-0.7113	0.0054-0.4504
0.8	T	0.5851-1.9680	0.2442-0.9192	0.1156-1.2943
	M	0.1452-1.6467	0.0163-3.0629	0.0187-0.6751
	B	0.0493-3.2151	0.0011-0.6123	0.0096-0.4909

Table 4 γ_{tv} for S2 (%) estimated from IP

SA	Loc	Cell Pressure (kPa) 50	100	200
2.4	T	0.0049-0.4747	0.0282-0.9028	0.0197-0.3953
	M	0.0147-0.8319	0.0216-0.8536	0.0072-0.7722
	B	0.0310-0.7378	0.0522-0.9129	0.0076-0.3258
1.6	T	0.0019-0.6675	0.0087-1.1841	0.0057-0.5601
	M	0.0042-1.6312	0.0011-1.0174	0.0045-0.4838
	B	0.0038-0.9827	0.0019-0.5110	0.0083-0.5805
0.8	T	0.0011-0.3402	0.0034-0.5605	0.0030-0.5794
	M	0.0023-0.8549	0.0019-1.5386	0.0008-0.5303
	B	0.0019-0.5144	0.0008-0.9354	0.0045-0.4112

Table 5 γ_{cl} for S1 (%) estimated from IP

SA	Loc	Cell Pressure (kPa) 50	100	200
2.4	T	0.2804-1.7204	0.0134-0.8547	0.1739-3.4617
	M	0.0646-1.1497	0.0061-1.8240	0.2332-1.4612
	B	0.0121-0.6603	0.0022-2.0432	0.0015-0.6380
1.6	T	0.0265-1.2563	0.0393-1.4275	0.0620-1.6479
	M	0.0238-1.6607	0.0151-1.2854	0.0261-0.9577
	B	0.0060-0.7540	0.0030-1.0280	0.0057-1.0473
0.8	T	0.02419-0.8761	0.0450-1.0730	0.0178-0.8338
	M	0.00794-1.9839	0.0094-1.3992	0.0094-0.5083
	B	0.00831-0.4566	0.0159-1.3005	0.0140-0.8141

Table 6 γ_{tv} and γ_{cl} for S1 (%) from LVDT

SA	γ_{tv} Cell Pressure (kPa) 50	100	200	γ_{cl} Cell Pressure (kPa) 50	100	200
2.4	0.0009	0.0542	0.0828	1.7180	1.7070	1.5062
1.6	0.0386	0.0359	0.0407	1.0876	1.1078	1.0769
0.8	0.0360	0.0451	0.0372	0.4868	0.3800	0.0439

Table 7 γ_{tv} and γ_{cl} for S2 (%) from LVDT

SA	γ_{tv} Cell Pressure (kPa) 50	100	200	γ_{cl} Cell Pressure (kPa) 50	100	200
2.4	0.0792	0.0892	0.054	1.5288	1.0169	1.3872
1.6	0.0046	0.0394	0.0659	0.5182	0.7583	0.9959
0.8	0.0184	0.0202	0.0315	0.4737	0.4855	0.9959

In order to verify the results from IP, the typical value of γ_{cl} was compared. The typical value ranges from 0.4-3% [8]. The minimum values for all conditions are within the range. On the other hand, the maximum values are larger. The LVDT results, as seen in Table 7, were also compared and a similar trend was observed. The results were also compared with the range of pore water pressure responses for sands with different relative densities proposed by Dobry (1985). The proposed range had an upper bound and lower bound curve as seen in Fig. 1. These were overlayed to the results of IP to investigate the validity of its results. Typical results are shown in Figs. 9-10. It can be seen that for S1 γ_c exceeds the boundary but for estimations prior to liquefaction. Once liquefaction had occurred the estimations are within the boundaries. For S2, more estimation can be seen within the boundary. More movements were present for S1 since it has more voids compared to S2. A difference can also be seen for the results of LVDT when it was compared with the proposed boundary. A smaller SA was used for the proposed boundary. The SA used had a maximum value of approximately 0.675% while a maximum value of 2.4% was used for the study.

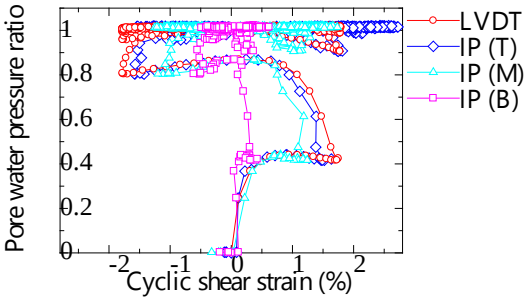

Fig.8 Comparison of the γ_c from LVDT and IP considering the sections monitored

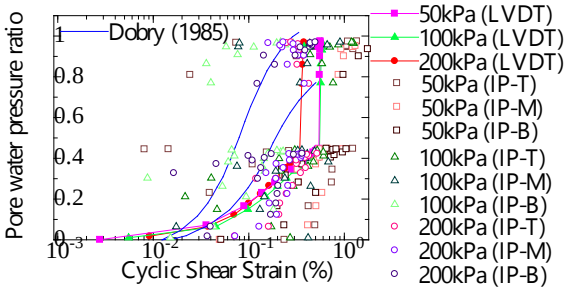

Fig.9 Comparison of the γ_c from LVDT and IP (S1)

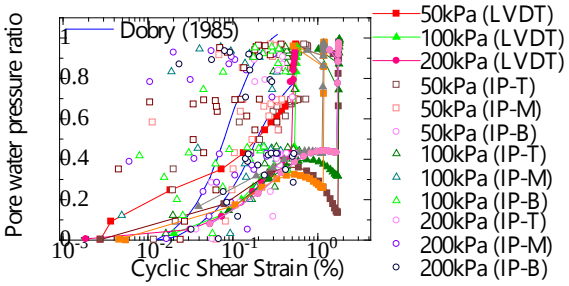

Fig.10 Comparison of the γ_c from LVDT and IP (S2)

6. CONCLUSION

Strain parameter-triggering liquefaction was estimated using a non-contact measurement technique. Before applying the technique, calibration was performed to eliminate the distortion from the lens and the scene. In addition to that, curvature correction was implemented with respect to the height of the sample, location, and section being monitored. The curved profile of the soil surface was corrected since it caused an error in the measurement of the deformation. Curvature correction can improve the monitoring of the mirrorless camera. The capacity of the mirrorless camera to estimate the cyclic shear strain was also investigated. The top cap was used as the target and it was compared with the LVDT. A good agreement was observed. For the internal measurement, a non-homogeneous deformation was observed. The values increased from the bottom to the top location. For the estimated γ_{tv}, no consistent trend was observed. Minimum values are within the typical values of 10^{-2}% or approximately $1x10^{-2}$%. Maximum values, on the other hand, are larger. For the estimated γ_{cl}, the relative density, strain amplitude and confining pressure. When the results are compared with the proposed boundary of Dobry (1985) it was also observed that the results were greatly affected by the value of SA used. The non-contact measurement technique implemented can still be extended to three-dimensional monitoring. This can be beneficial to understating the whole behavior of the soil as it experiences liquefaction.

7. ACKNOWLEDGMENTS

The researcher would like to express her gratitude to the Engineering Research and Development for Technology, Civil Engineering Department of De La Salle University and the Graduate School of Civil and Environmental Engineering of Nagoya University Geotechnical Engineering Division for their support.

8. REFERENCES

[1] Dungca, J.R., Kuwano, J., Takahashi, A, Saruwatari, T., Izawa, J., Suzuki, H. and Tokimatsu, K. Shaking table tests on the lateral response of a pile buried in liquid sand. Soil Dynamics and Earthquake Engineering, 2006, Vol. 26, Issue 2-4, pp. 287-295

[2] Dobry R. and Abdoun, T., Recent Findings on Liquefaction Triggering in Clean and Silty Sands during Earthquakes. Journal of Geotechnical and Geoenvironmental Engineering, Vol. 143, Issue 10, 2017, pp. 04017077-1-19.

[3] Dobry R. and Abdoun T., Cyclic Shear Strain Needed for Liquefaction Triggering and Assessment of Overburden Pressure Factor Kσ. ASCE Journal of Geotechnical and Geoenvironmental Engineering, 2015, pp. 1-18.

[4] Derakhshandi, M. et al. (2008). The effect of plastic fines on the pore pressure generation characteristics of saturated sands. Soil Dynamics and Earthquake Engineering, 28, 376–386.

[5] Kaddouri, A., Mechanical characterization of the threshold strain in sand liquefaction. Proceedings: Second International Conference on Recent Advances In Geotechnical Earthquake Engineering and Soil Dynamics. 1991, pp.2011-2014.

[6] Uy E.E.S. and Boonyatee T., Image Processing for Geotechnical Laboratory Measurements. International Journal of GEOMATE, Vol. 10, Issue 22, 2016, pp. 1964-1970.

[7] Longtan S., Song Y., Yong S., Chuan, H. and

Xiaoxia, G., Application of Digital Image Processing Technology in Dynamic Triaxial Test of Soil Mechanics. Journal of Theoretical and Applied Information Technology, Vol. 48, Issue 3, 2013, pp.1358-1365.

[8] Koseki J., Hoshino R., Miyashita Y. and Sato T., Direct and Indirect Observations of Local Properties of Saturated Sand Specimens in Undrained Cyclic Triaxial Tests. The 6th Japan-Korea Geotechnical Workshop, Vol. 4, Issue 1, 2016.

[9] Wahyudi S., Miyashita Y. and Koseki, J. Shear Banding Characteristics of Sand in Torsional Shear Test Evaluated By Means of Image Analysis Technique, Bulletin of ERS, No.45, 2012, pp.1-8

[10] Fernando W.S.P., Udawatta L., and Pathirana P., Identification of Moving Obstacles with Pyramidal Lucas and Kanade Optical Flow and K Means Clustering. Proceedings of the Third International Conference on Information and Automation for Sustainability, 2007.

[11] Thota S.D., Vemulapalli K.S., Chintalapati K. and Srinivas, P.S., Comparison Between the Optical Flow Computational Techniques. International Journal of Engineering Trends and Technology, Vol. 4, Issue 10, 2013.

[12] The Japanese Geotechnical Society, Japanese Geotechnical Society Standards: Laboratory Testing Standards of Geomaterial. Issue 1, 2008.

[13] Sutton M.A., Orteu J.J., and Schreier H.W., Image Correlation for Shape, Motion and Deformation Measurements: Basic Concepts, Theory, and Applications: Springer, 2009. Vol.25, No.3, 2011, pp.1460-1465.

[14] Dobry R. and Abdoun T., An Investigation into Why Liquefaction Charts Work: A Necessary Step Toward Integrating the States of Art and Practice. Proceedings of the Fifth International Conference on Earthquake Geotechnical Engineering,2011,pp.13-45.